Bulletin of the Seismological Society of America, Vol. 104, No. 5, pp. –, October 2014, doi: 10.1785/0120140062

Ⓔ

Moment Magnitude–Rupture Area Scaling and Stress-Drop Variations for Earthquakes in the Mediterranean Region

by K. I. Konstantinou

Abstract A dataset of moment magnitudes and rupture areas is compiled for 53 earthquakes that occurred in the Mediterranean region during the period 1976–2013. Moment magnitudes of these events range from 4.45 to 7.56, and the rupture areas are mainly inferred from the dimensions of their aftershocks zone. Three magnitude–area relationships that have been determined using global datasets, namely Wells and Coppersmith (1994), Hanks and Bakun (2002), and Shaw (2009), are examined to determine how well they fit these observations. The relationship of Shaw (2009) exhibits the best goodness of fit to the data, followed very closely by a modified version of the Hanks and Bakun bilinear relationship. Statistical tests show that the magnitude residuals of the two relationships are not significantly different, thus either of them could be used for seismic-hazard analysis. Stress drop of the selected events varies within a narrow range, increasing from 1 MPa for seismic moments less than 1×10^{18} N·m to about 6 MPa for larger events. Taking into account that the majority of the events under study are either normal or strike-slip earthquakes, this pattern of stress-drop variation is in contrast to that in areas like Taiwan or the Mexico subduction zone, where thrust faulting is dominant. For these areas, earthquakes tend to exhibit larger stress drops of up to 100 MPa, suggesting there is an apparent dependence of stress-drop variation on faulting type.

Online Material: Detailed information for 53 earthquakes used to derive the magnitude–rupture area scaling relation.

Introduction

The first step in any seismic-hazard analysis is the identification of potential seismogenic faults and the evaluation of all moderate and large ($\mathbf{M} \geq 5$) earthquakes they may generate (Mohammadioun and Serva, 2001). This evaluation can be done using either macroseismic intensities or empirical relationships that connect the magnitude with rupture length, which can be measured from field/seismological observations. Wyss (1979) argued that the use of rupture length for evaluating potential earthquake magnitude results in less accurate estimates, because a long and thin fault can release less elastic energy than its long and wide counterpart. In this sense, an empirical relationship linking magnitude with rupture area A (the product of fault length L and width W) would produce more accurate estimates. In the past, several such magnitude–rupture area relationships have been proposed using global and regional datasets of fault dimensions derived from aftershock area distributions, geological mapping of faults, and more lately from finite-fault models (Stirling *et al.*, 2013, and references therein).

Moment magnitude–rupture area scaling is influenced by the assumption of whether stress drop from the smaller to larger magnitude earthquakes can be considered as constant or not. For a shear crack, the average static stress drop $\Delta\sigma$ can be defined as (Lay and Wallace, 1995)

$$\Delta\sigma = C\mu\frac{D}{\Lambda}, \tag{1}$$

in which D is mean slip, Λ is the smallest dimension of rupture, μ is the rigidity modulus, and C is a constant dependent on rupture geometry. If constant stress drop is assumed, then this equation predicts that, for earthquakes with rupture length smaller than their width, the mean slip should increase and approach a constant value when the width becomes comparable to the thickness of the seismogenic layer (the W-model according to Scholz, 1982). On the other hand, if stress drop is not considered constant, then mean slip would linearly relate to rupture length L (the L-model according to Scholz, 1982). The debate over which of the two models better describes the mechanics of rupture has been ongoing for over three decades, with neither model being widely accepted (Scholz, 1982; Romanowicz, 1992; Bodin and Brune, 1996;

Pegler and Das, 1996; King and Wesnousky, 2007; Shaw and Wesnousky, 2008).

The Mediterranean region encompasses three plate boundary types: subduction zones (Hellenic, Tyrrhenian, Cypriot), collision zones (Morocco, Algeria, Adriatic), and transform faults (North Anatolian and Dead Sea faults). All of these are characterized by significant seismogenic potential as manifested by numerous destructive earthquakes that have occurred in the past and devastated densely populated cities, such as the 1999 İzmit and Athens earthquakes or the 2009 L'Aquila earthquake. Even though the possibility of a large megathrust earthquake along one of the subduction zones in the Mediterranean cannot be discarded (Sørensen *et al.*, 2012), it is the smaller and more numerous events on land that constitute the main source of seismic hazard in the region. Greece, Italy, and Turkey exhibit the bulk of this seismicity and have developed dense seismic networks for monitoring and early warning purposes (e.g., Melis and Konstantinou, 2006). This has the consequence that even moderate-to-small magnitude (≤ 5) events can be studied and their fault dimensions determined from their early aftershocks distribution.

This work aims at investigating the scaling relationship between moment magnitude **M** and rupture area A in the Mediterranean region by utilizing a set of rupture area dimensions of 53 earthquakes. In the first part of the paper, a description is given of the methodology used to decipher the individual fault dimensions (L,W) for each of the 53 events considered. This is followed by an evaluation of how well this dataset is fit by existing scaling relationships, namely those proposed previously by Wells and Coppersmith (1994), Hanks and Bakun (2002, 2008), and Shaw (2009). Stress-drop variations of these earthquakes are also examined; and, for seismic moment smaller than 1×10^{18} N·m, the stress drop is around 1 MPa, increasing to 6 MPa for larger values of moment. This behavior is discussed and compared with stress-drop observations from two other regions, the Taiwan collision zone and the Mexican subduction zone.

Data Selection

Studies of aftershock sequences of 53 earthquakes that occurred in regions around the Mediterranean Sea between 1976 and 2013 have been used to infer the rupture area dimensions primarily from the extent of their aftershock zone (Fig. 1). The majority of these events had a hypocentral depth of 15 km or less, and the depth of the deepest event did not exceed 32 km. Most of the events included in the dataset comply with the following criteria: (1) aftershocks were recorded by a dense regional or local network with a good azimuthal coverage and (2) the location errors (horizontal and vertical) were less than 5 km on average and less than 3 km for the majority of the events. The total duration of the recording period of the aftershock sequence was another factor that was taken into account, as aftershock area expansion may result in significant overestimation of the coseismic rupture area. It should also be noted that seismological data of earthquakes that occurred in the late 1970s through the 1980s and 1990s were subsequently reprocessed using modern techniques, such as the double-difference relocation method (Waldhauser and Ellsworth, 2000). This has resulted in higher-resolution estimates of aftershock locations and corresponding fault dimensions than previously available for a number of events (examples of such cases are the 1976 Friuli in Italy and the 1995 Kozani–Grevena earthquake in Greece).

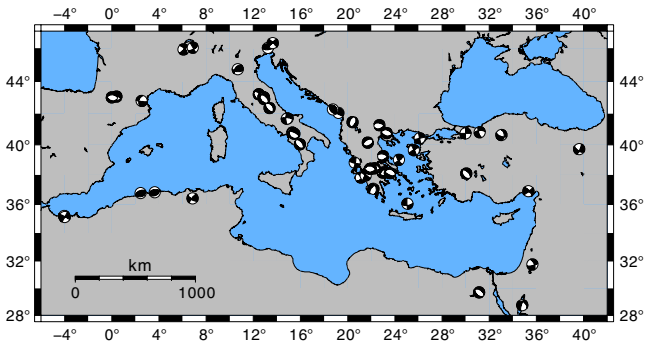

Figure 1. The broader Mediterranean area, showing the locations and focal mechanisms of the 53 earthquakes considered in this study (for individual source parameters, see Table 1). The color version of this figure is available only in the electronic edition.

For many of the selected events, additional studies are available in which the seismogenic fault is studied in the context of finite-fault models or by using geodetic observations such as leveling, Global Positioning System, and/or Interferometric Synthetic Aperture Radar (InSAR). These studies were also taken into account when determining the rupture area, especially in the cases in which aftershock zone expansion or static triggering of secondary faults was considered probable. Following are three examples of such events.

- The 17 August 1999 İzmit, Turkey, earthquake ruptured a large segment of the North Anatolian fault, and its rupture process has been the topic of several studies. These studies seem to exhibit significant differences in the rupture length, with the fault length inferred from aftershocks. More recently, Yalcinkaya *et al.* (2012) performed an evaluation of all published finite-fault models by stochastic simulations in order to predict peak ground motions at nearby strong-motion stations. The authors find optimal fitting between synthetics and observations for fault dimensions $L = 150$ km and $W = 18$ km, which also coincide with the results of the finite-fault study of Bouchon *et al.* (2002), and these were adopted here.
- The 7 September 1999 Athens, Greece, earthquake ruptured a previously unknown fault, causing casualties and significant damage to the nearby Athens metropolitan area. Although aftershock studies give rupture length 20–25 km and down-dip width between 14 and 16 km, the finite-fault model of Baumont *et al.* (2004) derived from the inversion of strong-motion and InSAR data exhibits significant slip at depths larger than that of the located aftershocks (i.e.,

below the brittle–ductile boundary). In order to correctly determine the coseismic rupture area, this study adopts the finite-fault model dimensions, which are $L = 15$ km and $W = 17$ km.

- The 14 August 2003 Lefkada, Greece, earthquake ruptured two segments of the Cephalonia Transform fault in the Ionian Sea. Detailed analysis of the aftershock sequence and the rupture process of the mainshock indicate that the earthquake consisted of two subevents separated in space by 40 km and in time by 14 s (Zahradnik *et al.*, 2005; Benetatos *et al.*, 2007). Static stress triggering of the second subevent has been invoked, therefore this study adopts the fault dimensions of the first subevent ($L = 25$ km, $W = 10$ km) and its corresponding seismic moment (1.5×10^{18} N·m).

In general, when there was a discrepancy between aftershock zone dimensions and dimensions obtained by other means, higher weight was given to studies that utilized multidisciplinary modeling of seismological and geodetic observations to infer the rupture area.

Seismic moment values for most events were adopted from the individual studies and were derived from the inversion of teleseismic *P*, *SH* waveforms, or regional waveform data; M_0 estimates were taken from the Global Centroid Moment Tensor or the Swiss Seismological Service moment tensor catalogs for only seven events. For reasons of consistency, seismic moment was then used to calculate moment magnitude according to the equation of Hanks and Kanamori (1979):

$$\mathbf{M} = \frac{2}{3}\log M_0 - 10.7. \tag{2}$$

In cases in which several moment estimates of the same event were available (from the individual aftershock study, spectral analysis, finite-fault modeling, moment tensor catalogs), the differences in moment magnitude were assessed; and, on average, they were up to 0.15 units. Focal mechanisms were available for all events: in the majority of the cases, they were determined by waveform inversion and, in the case of smaller earthquakes, from *P*-wave polarities. All events were finally classified as strike slip (SS) or dip slip (DS) according to the value of the rake of the nodal plane corresponding to the seismogenic fault. Table 1 gives a summary of the fault dimensions, rupture areas, and seismic moments of the 53 events included in this study. The overlap of this dataset with that of Wells and Coppersmith (1994) is only 10 events (21%), whereas 32 events (60%) exhibit DS faulting mechanism and 21 events (39%) are SS earthquakes. Ⓔ A description of all available information for each earthquake can be found in the electronic supplement that accompanies this paper.

Scaling Relationships

A global dataset of 148 earthquake fault dimensions was used by Wells and Coppersmith (1994) to derive scaling relationships between moment magnitude and rupture area. These relationships have been utilized extensively throughout the world in seismic-hazard analysis studies for the purpose of predicting magnitudes of expected earthquakes. The linear regression relationship (hereafter referred to as WC94) for all rupture area data independent of faulting type is given by

$$\mathbf{M} = 0.98 \log A + 4.07. \tag{3}$$

This relationship is valid for moment magnitudes in the 4.7–8.6 range. Separate relationships have been derived for SS and DS events, even though the authors note that the results obtained from these were not significantly different in a statistical sense.

Hanks and Bakun (2002) used a subset of this dataset (83 strike-slip earthquakes) and showed that the previous relationship can only fit well for events with rupture areas equal to or smaller than 537 km^2 ($\mathbf{M} \leq 6.71$), while there was a magnitude underestimation for larger events. Instead, the authors proposed a bilinear relationship in which the first branch (events smaller than 6.71) would have a constant stress drop $\Delta\sigma$ of 2.6 MPa, thus

$$\mathbf{M} = \log A + \frac{2}{3}\log \Delta\sigma - 10.9958 = \log A + 3.98. \tag{4}$$

The second branch would include events larger than 6.71 and follow an L model of the form $\bar{u} = \alpha L$ (thus assuming nonconstant stress drop for larger earthquakes), in which $\bar{u}$ is mean displacement and $\alpha = 2 \times 10^{-5}$. The relationship would then be given by

$$\mathbf{M} = \log A + \frac{2}{3}\log\left(\frac{\mu\alpha}{W}\right) - 10.7 = \frac{4}{3}\log A + 3.03, \tag{5}$$

for $\mu = 3 \times 10^{11}$ dyn·cm^{-2} and $W = 16$ km, proportional to the average thickness of the seismogenic layer worldwide. This bilinear relationship will be hereafter referred to as HB02. Subsequently, Hanks and Bakun (2008) included seven more large strike-slip events in an effort to ascertain the robustness of their scaling relationship and found that their initial results were unchanged.

On the other hand, Shaw (2009) argued that a scaling law that assumes constancy of stress drop over the whole magnitude range and that also includes the geometrical effects of the finite seismogenic layer can match the data of Hanks and Bakun better. The relationship suggested by Shaw (2009; hereafter referred to as S09) is of the form

$$\mathbf{M} = \log A + \frac{2}{3}\log\frac{\max\left(1, \sqrt{\frac{A}{H^2}}\right)}{\left[1 + \max\left(1, \frac{A}{H^2\beta}\right)\right]} + \text{const}, \tag{6}$$

in which H is the thickness of the seismogenic layer and the parameter β signifies the additional slip in the seismogenic

Table 1
List of Earthquakes and Corresponding Source Parameters that Have Been Included in This Study

Event Number	Date (yyyy/mm/dd)	Latitude (°)	Longitude (°)	H (km)*	M_w	M_0 (N·m)	L (km)	W (km)	A (km^2)
1	1976/05/06	46.02	13.24	7.5	6.51	6.60×10^{18}	25	15	375
2†	1978/06/20	40.76	23.30	8	6.44	5.13×10^{18}	28	14	392
3	1979/04/15	42.04	19.21	7	7.06	4.38×10^{19}	50	23	1150
4	1979/05/24	42.26	18.75	6	6.20	2.24×10^{18}	17	11	187
5†	1980/02/29	43.07	0.400	4	5.16	6.36×10^{16}	5	5	25
6†	1980/07/09	39.25	23.01	17	6.59	8.67×10^{18}	30	13	390
7	1980/11/23	40.79	15.31	11	6.91	2.60×10^{19}	50	14	700
8	1981/02/24	38.16	22.97	12	6.57	8.10×10^{18}	28	17	476
9	1981/03/04	38.18	23.17	4	6.23	2.49×10^{18}	25	10	250
10†	1984/04/29	43.21	12.46	7	5.65	3.40×10^{17}	14	6	84
11†	1985/10/27	36.42	6.85	10	5.77	5.20×10^{17}	14	10	140
12	1986/09/13	37.06	22.18	5	5.86	7.00×10^{17}	10	10	100
13	1989/10/29	36.78	2.44	11	5.90	8.20×10^{17}	13	10	130
14	1992/03/13	39.71	39.62	8.7	6.66	1.10×10^{19}	30	10	300
15	1992/10/12	29.71	31.14	23	5.95	9.70×10^{17}	12	10	120
16	1994/05/26	35.20	−4.03	8	5.86	7.10×10^{17}	16	8	128
17	1995/05/13	40.14	21.71	13	6.74	14.5×10^{18}	28	10	280
18	1995/06/15	38.45	22.29	7	6.32	3.40×10^{18}	27	11	297
19	1995/10/01	38.10	30.05	7.5	6.26	2.80×10^{18}	24	12	288
20	1995/11/22	28.76	34.80	13	7.21	7.42×10^{19}	48	24	1152
21	1996/02/18	42.79	2.53	8	5.12	5.40×10^{16}	5	7	35
22	1996/04/03	40.71	15.48	8	5.09	5.00×10^{16}	9	4	36
23	1996/07/15	45.93	6.08	2	4.76	1.55×10^{16}	2.5	4	10
24	1996/10/15	44.74	10.68	15	5.39	1.40×10^{17}	9	5	45
25	1997/09/26	43.03	12.86	5.7	5.67	3.70×10^{17}	7	4	28
26	1997/09/26	43.02	12.89	5.7	5.90	8.10×10^{17}	12	5	60
27	1997/10/14	42.91	12.92	5.9	5.65	3.40×10^{17}	7	4	28
28	1998/04/12	46.30	13.65	7.6	5.73	4.50×10^{17}	13	7	91
29	1998/06/27	36.90	35.32	32	6.33	3.63×10^{18}	30	18	540
30	1998/09/09	40.03	15.95	10	5.43	1.57×10^{17}	9	6	54
31	1999/08/17	40.73	29.99	17	7.56	2.50×10^{20}	150	18	2700
32	1999/09/07	38.12	23.58	9.5	6.10	1.60×10^{18}	15	17	255
33	1999/11/12	40.81	31.19	11	7.11	5.26×10^{19}	55	17	935
34	2000/06/06	40.63	33.03	5	5.96	1.00×10^{18}	13	8	104
35	2001/07/26	39.01	24.35	12	6.45	5.43×10^{18}	27	14	378
36	2002/10/31	41.69	14.91	16	5.79	5.46×10^{17}	6	13	78
37	2002/11/01	41.68	14.84	18	5.66	3.58×10^{17}	8	8	64
38	2002/12/02	37.83	21.12	17	5.48	1.89×10^{17}	5	6	30
39	2003/05/21	36.83	3.65	10	6.94	2.89×10^{19}	50	15	750
40	2003/07/06	40.42	26.10	18	5.68	3.77×10^{17}	10	6	60
41	2003/08/14	38.82	20.60	10	6.08	1.50×10^{18}	25	10	250
42†	2004/02/11	31.75	35.66	18	5.29	9.97×10^{16}	8	7	56
43	2004/02/24	35.12	−3.99	6	6.35	3.80×10^{18}	19	12	228
44†	2005/09/08	46.03	6.88	4.3	4.47	5.74×10^{15}	2.5	2	5
45	2006/11/17	43.02	0.00	9.7	4.45	5.32×10^{15}	2	4	8
46	2008/06/08	37.97	21.52	22	6.40	4.49×10^{18}	30	10	300
47	2009/04/06	42.35	13.38	9.5	6.32	3.50×10^{18}	25	12	300
48	2009/05/24	41.26	22.69	7	5.18	6.74×10^{16}	6	6	36
49	2009/09/06	41.46	20.41	6	5.39	1.38×10^{17}	9	6	54
50	2010/01/18	38.41	21.91	6.6	5.29	9.70×10^{16}	6	6	36
51	2010/01/22	38.42	21.96	8.0	5.19	7.00×10^{16}	6	5	30
52	2012/01/27	36.04	25.06	14	5.38	1.33×10^{17}	8	6	48
53	2013/01/08	39.64	25.61	11	5.83	6.40×10^{17}	10	8	80

*H signifies the hypocentral depth of each event as has been determined by the published studies.
†Individual events for which the seismic moment value is adopted from either the Global Centroid Moment Tensor or Swiss Seismological Service moment tensor catalogs.

layer due to increased fault width W, as well as the additional moment released below the seismogenic layer. The value of the constant term is set by fitting at the small events. In the next section, the fitting of these scaling relationships to the compiled dataset of Mediterranean earthquakes will be examined on a statistical basis.

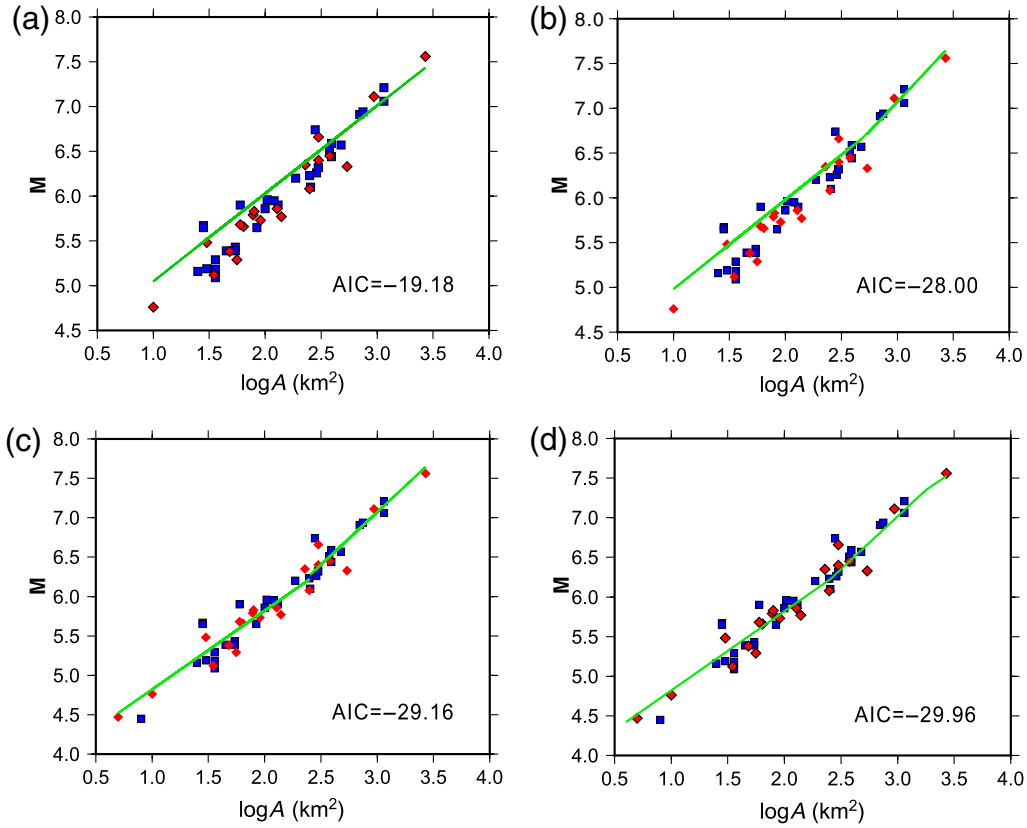

Figure 2. Diagrams that show the fit of the scaling relationships suggested by (a) Wells and Coppersmith (1994), (b) Hanks and Bakun (2002), (c) this study, and (d) Shaw (2009) to the **M**– log A observations included in this study. The squares represent dip-slip (DS) events, and the diamonds correspond to strike-slip (SS) earthquakes. The goodness of fit for each relationship is given by the Akaike information criterion (AIC) value shown in the lower right corner of each plot. The color version of this figure is available only in the electronic edition.

Model Fitting

The estimated rupture areas, when plotted against moment magnitude, produce a coefficient of determination indicative of a highly linear cluster of values ($R^2 = 0.92$; Fig. 2). The goodness of fit between the aforementioned scaling relationships and the data is quantified by estimating the Akaike information criterion (AIC; Akaike, 1974). For this study, the AIC is given by

$$\mathrm{AIC} = n[\ln(2\pi\sigma^2) + 1] + 2k, \qquad (7)$$

in which n is the number of observations, σ is the standard deviation of the magnitude residuals, and k is the number of free parameters involved in each relationship ($k = 2$ for WC94 and HB02; $k = 3$ for S09). The AIC is founded on the concept of information entropy, offering a relative estimate of the information lost when a given model is used to represent the process that generates the data. As it is expressed, the AIC not only rewards the goodness of fit of a particular model, but also includes a penalty that is an increasing function of the number of estimated parameters. The model that attains the smallest AIC value is then considered as the most suitable.

Initially, the fitting of the WC94 and HB02 scaling relationships was examined after removing the two smallest events ($\mathbf{M} \sim 4.5$) of the dataset, because the magnitude range of their validity was between 4.7 and 8.6 (Wells and Coppersmith, 1994). It is evident that the WC94 relationship underestimates the larger events ($\mathbf{M} > 6.6$), as Hanks and Bakun (2002) had already noticed, and at the same time overestimates the magnitudes of the smaller events (Fig. 2a). The corresponding residuals shown in Figure 3a suggest that the standard deviations for DS and SS events are of similar amplitude. As expected, the HB02 bilinear relationship is doing much better for the larger events; however, it still significantly overestimates the magnitudes of the smaller ones (Figs. 2b and 3b) because it is essentially the same as the WC94 relationship. In order to improve the fit for the smaller events, the coefficient of log A is kept equal to 1.0 and the intercept value is determined using a least-squares fit. This calculation yields an intercept value of 3.82, which also changes the crossover point of the two linear branches from 537 to 251 km^2, corresponding to a 6.3 moment magnitude. In this way, the modified scaling relationship for $A \le 251$ km^2 becomes $\mathbf{M} = \log A + 3.82(\pm 0.02)$. The fit can be seen in Figure 2c, whereas the residuals distribution in Figure 3c

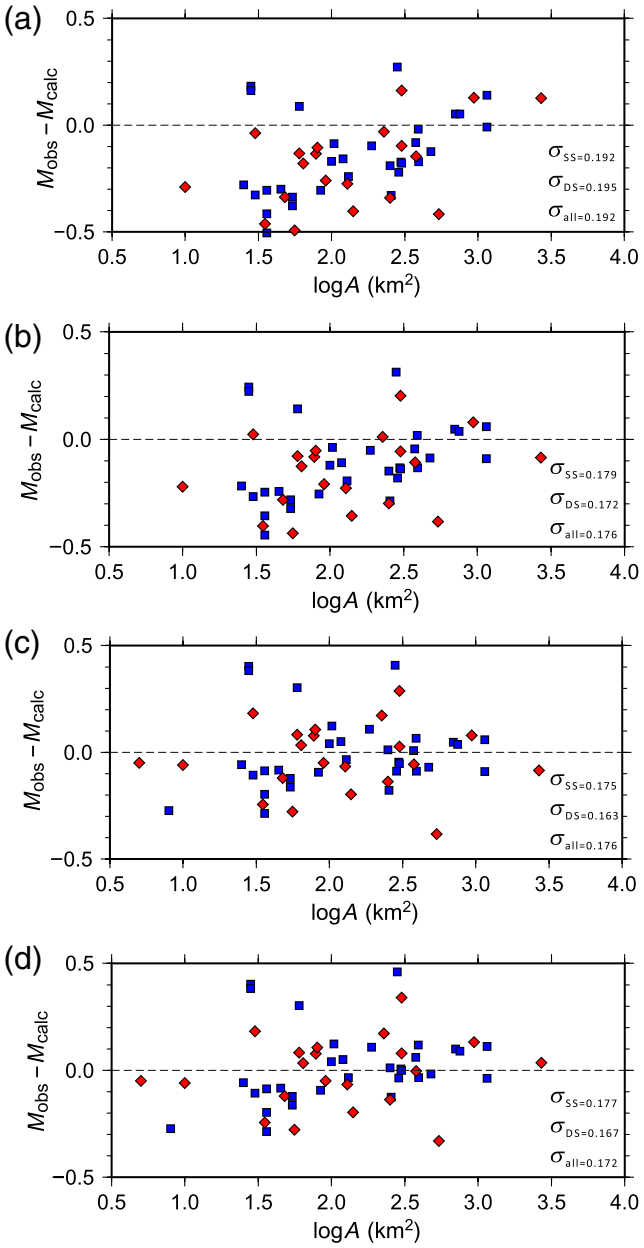

Figure 3. Plots of the magnitude residuals between observed and calculated magnitudes derived from the relationships of (a) Wells and Coppersmith (1994), (b) Hanks and Bakun (2002), (c) this study, and (d) Shaw (2009). The symbols σ_{DS} and σ_{SS} represent the standard deviation of the residual for DS and SS events, respectively, whereas σ_{all} stands for the standard deviation of all residuals. All other symbols are the same as in Figure 2. The color version of this figure is available only in the electronic edition.

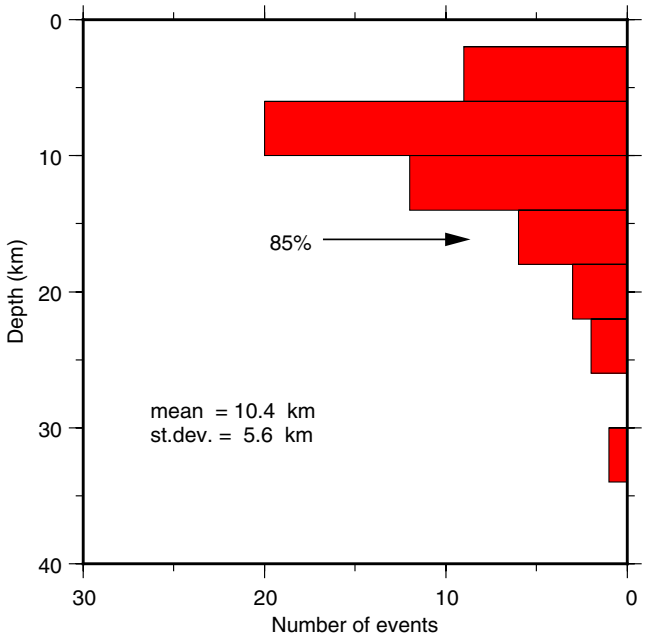

Figure 4. The distribution of hypocentral depth for the 53 events under study. The bin width is 5 km, which is representative of the largest vertical error. Also shown is the percentage of events within 16 km depth, along with the mean and standard deviation of all the depth values. The color version of this figure is available only in the electronic edition.

exhibits a much more symmetric pattern and standard deviations smaller than previously observed.

The S09 scaling relationship is then examined for its goodness of fit by substituting the constant term with the intercept value determined earlier. The two additional parameters H and β were previously determined by Shaw (2009) as $H = 16$ km and $\beta = 6.9$ for a global dataset of strike-slip events. These values are also adopted in this study for the following reasons:

- The majority (85%) of the events included in the dataset of Mediterranean earthquakes nucleated at depths $\leq$16 km. This can be clearly seen in Figure 4, where the distribution of nucleation depths for the 53 events is shown. This value also represents the mean value of the depths plus one standard deviation (10.4 + 5.6 km).
- Shaw (2009) determined one standard deviation error bars for the parameter β (between 5.4 and 9.9) using a likelihood function and assuming Gaussian errors. By varying β within this interval, it is found that the changes in the data fit are insignificant.

Figures 2d and 3d show that, graphically, the fit of S09 is as good as that of the modified bilinear relationship, whereas its AIC value is the smallest of all models considered. However, its difference with the modified bilinear model is only marginal, as indicated by the high relative probability of the two models ($e^{\Delta AIC/2}$), and is equal to 0.67 (67%). This means the modified bilinear relationship is 67% as probable as the S09 model to minimize the information loss. It is also worth noting that the standard deviations of magnitude residuals for DS and SS events are the smallest for the bilinear model. Two statistical tests were performed to infer whether the magnitude residual distributions of the two models are significantly different. The first is an F-test for significantly different variances, which showed the two residual variances were not significantly different for a confidence level of

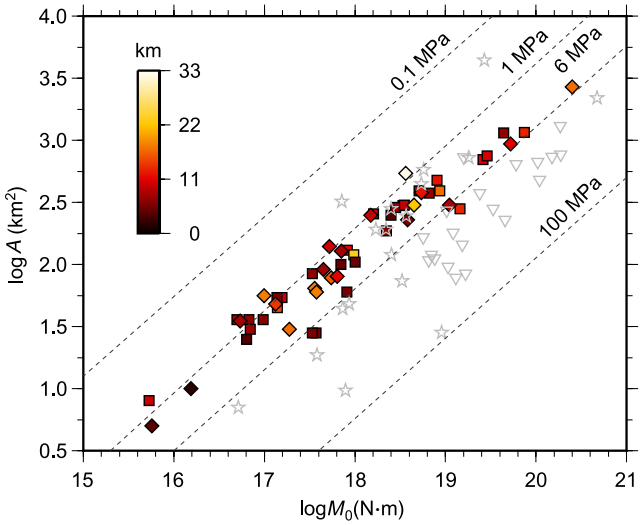

Figure 5. A comparison of the logarithm of seismic moment versus the logarithm of rupture area for the 53 events that occurred in the Mediterranean region and other areas. The squares represent DS events and the diamonds SS earthquakes, and the shading gradient indicates the depth of the events as shown in the legend. Stars represent observations of earthquakes in Taiwan (Yen and Ma, 2011), whereas the inverted triangles are observations of earthquakes that occurred along the Mexico subduction zone (Rodriguez-Péres and Ottomöller, 2013). The color version of this figure is available only in the electronic edition.

95% (p-value $= 0.8542 > 0.05$). The second test is the nonparametric Kolmogorov–Smirnov test, which tests the hypothesis of whether two samples are drawn from the same continuous population. The results show that the null hypothesis of having the same population for the two residual samples cannot be rejected at a confidence level of 95% (p-value $= 0.997 > 0.05$). On statistical grounds, it is not possible to unambiguously infer that the S09 model fits the observations significantly better than a bilinear model.

Stress-Drop Variations

The smaller intercept value derived for the modified HB02 scaling relationship implies that the average stress drop for the Mediterranean earthquakes with $\mathbf{M} \leq 6.3$ is 1.5 MPa. This is smaller than the commonly quoted average stress-drop value of 3 MPa or the one assumed by Hanks and Bakun (2002) of 2.6 MPa. Questions that naturally arise then are: (1) What is the behavior of stress drop as a function of seismic moment and does this behavior agree with $\Delta\sigma$ estimates determined from strong-motion recordings? and (2) How does the stress-drop variation in the Mediterranean region compare with that in other areas? For the purpose of investigating these points further, a plot of the logarithms of rupture area and seismic moment for the 53 Mediterranean earthquakes is superimposed on isolines of 0.1, 1.0, 6.0, and 100 MPa, corresponding to calculated stress drops for a circular crack model (Fig. 5). The seismic moment and rupture areas of earthquakes that occurred along the Mexico subduction zone (Rodriguez-Pérez and Ottomöller, 2013) and in the Taiwan collision zone (Yen and Ma, 2011) are also plotted for comparison purposes. The reasoning behind the choice of these two regions stems from the facts that reliable rupture areas and M_0 estimates derived from finite-fault modeling were available and they represent two tectonic regimes where thrust faulting is dominant.

For seismic moment values in the range of 1×10^{15}–1×10^{18} N·m, the majority of the Mediterranean events lie close to the 1.0 MPa isoline, whereas the events with larger M_0 gradually approach the 6.0 MPa isoline. Exceptions to this pattern are three events with released moment smaller than 1×10^{18} N·m that exhibit stress drops on the order of 6.0 MPa; these events correspond to the earthquakes that occurred in 1997 in Umbria, Italy (events 25, 26, and 27 in Table 1). The other two earthquakes that appear to have stress drops slightly higher than 6 MPa are the 1992 Erzincan, Turkey, and 1995 Kozani–Grevena, Greece, events (number 14 and 17 in Table 1, respectively). Previously it had been suggested that deeper events may attain larger stress-drop values (Hardebeck and Aron, 2009); however, this does not seem to be the case for the Mediterranean earthquakes considered here. In fact, the 1998 Adana earthquake in Turkey (event 29 in Table 1), which is the deepest event in the dataset (~32 km), exhibits a relatively low stress drop of about 1.0 MPa. Similar observations of no increasing stress drop with nucleation depth have been also reported for a global dataset studied by Allmann and Shearer (2009).

Independent estimates of stress drop for some of the events included in this study have been obtained previously by analyzing acceleration spectra and/or spectral ratios. More specifically, stress-drop estimates of three Greek earthquakes (the 1978 Thessaloniki, 1981 Corinth, and 1995 Kozani–Grevena earthquakes; events 2, 8, and 17 in Table 1) have been published by Margaris and Boore (1998). Their analysis revealed stress-drop values of 5.4, 4.8, and 6.3 MPa for these three earthquakes, respectively, consistent with what is expected from Figure 5. A similar analysis of the 2002 Molise earthquakes in Italy (events 36 and 37 in Table 1) shows that they attained stress drops of 2 MPa (Calderoni *et al.*, 2010), again in good agreement with the results presented here. A stress-drop value of 7 MPa has also been determined for the Düzce earthquake (event 33) by Umutlu *et al.* (2004), which is about 1 MPa higher than what is obtained in this study. Rovelli and Calderoni (2014) showed that the Umbria mainshock earthquakes have stress drops on the order of 5 MPa, which is quite close to the value of 6 MPa inferred from Figure 5. It is worth mentioning that the relatively higher stress drop of the Umbria events compared with other earthquakes of similar magnitude may be a result of fault zone properties. Manighetti *et al.* (2007) suggested that stress drop is a function of the structural maturity of a given fault, defining as mature faults those with clear surface expression, large rupture lengths, and an age of several million years. In this sense, mature faults are weakened zones that rupture in lower stress-drop earthquakes. It therefore is

possible that the Umbria earthquakes may have occurred along structurally immature faults, a suggestion that is supported by the fact that these faults were blind normal faults of relatively small length (Chiaraluce *et al.*, 2003).

A comparison of stress-drop variations of the Mediterranean events with the other two areas (Mexico and Taiwan) shows one important difference. The Taiwanese earthquakes exhibit an inverse relationship of high stress drop (6–100 MPa) for small and moderate events and a gradual decrease for very large events (down to less than 1 MPa). On the other hand, the earthquakes occurring along the Mexican subduction zone show a similar trend of decreasing stress drop with increasing seismic moment, even though their M_0 range is more limited. One reason for this difference may be the dominant faulting style in each of these datasets. The majority of events in Mexico and Taiwan represent low-angle thrust faulting mechanisms, whereas most events in the Mediterranean are normal-faulting earthquakes. Indeed, Allmann and Shearer (2009) observed that thrust faults show an apparent decrease of stress drop with increasing M_0, in contrast to their normal/strike-slip counterparts. This agrees well with the observations presented here, in the sense that stress drop of thrust faulting events in Taiwan and Mexico appears to have an inverse variation as a function of moment than the stress drop variation exhibited by the normal/strike-slip earthquakes in the Mediterranean.

Conclusions

The Mediterranean region is a seismically active area in which the main seismic hazard stems from earthquakes with moment magnitudes on the order of 6.5 or smaller. A well-calibrated magnitude–rupture area relationship is therefore essential in the effort to estimate the magnitude of future earthquakes and for predicting the characteristics of the expected ground motion. The dataset of 53 moment magnitudes and rupture areas compiled in this study can be adequately fit by the S09 relationship with $H = 16$ km and $\beta = 6.9$ or by a bilinear scaling relationship of the form

$$\mathbf{M} = \log A + 3.82(\pm 0.02), \qquad A \leq 251 \text{ km}^2 \qquad (8)$$

and

$$\mathbf{M} = \frac{4}{3}\log A + 3.07(\pm 0.04), \qquad A > 251 \text{ km}^2, \qquad (9)$$

which is a modification of the HB02 relationship proposed for a global dataset of strike-slip earthquakes. Although the S09 model shows a marginal superiority over the bilinear relationship, the magnitude residuals of the two models are not significantly different in a statistical sense. From the practical point of view, either of them could be used in seismic-hazard analysis; however, the general tendency among scientists would be to use the model with the smallest number of free parameters. This consideration would undoubtedly favor the bilinear model. Another complication regarding the use of the S09 relationship is that it implicitly assumes that every earthquake should exhibit an amount of deep slip; however, such an assumption is in most cases difficult to validate for any particular earthquake. The results of this study also cast doubt on the practice of using the (still) popular WC94 relationship, or in fact any global scaling relationship for which the goodness of fit to the regional observations has not been critically examined.

Stress drop in the Mediterranean region seems to vary within narrow limits (1–6 MPa) and could be considered to first order as independent of seismic moment. A similar trend has been reported earlier by Hofstetter and Shapira (2000), who determined stress-drop estimates for a number of earthquakes in the eastern Mediterranean. This behavior is in contrast to what is observed for events of similar magnitude occurring in the Taiwan collision zone and along the Mexican subduction zone, where stress-drop variations are larger (1–100 MPa) and follow a pattern of decreasing stress drop with increasing seismic moment. The primary cause of this difference may be the dominant faulting style in each area, which is normal/strike slip for the Mediterranean and thrust faulting in the other two regions.

Finally, it is important to view the results of this study in light of the scaling-law classification scheme suggested recently by Stirling *et al.* (2013), who also ranked previously published relationships based on their quality and quantity of the regression dataset. Following this scheme the $\mathbf{M}$– $\log A$ scaling relationships developed in this study can be applied in fast (> 10 mm/yr) plate boundary settings and in particular for normal and/or strike-slip faults. They also fulfill two other quality-control criteria that Stirling *et al.* (2013) have set: the dataset size and the inclusion of data that span the last 10–20 years. The rupture areas compiled in this study and the derived scaling relationships fill an important gap in the earthquake scaling law literature, in both a regional sense and as a tool to further understand fault-rupture mechanics.

Data and Resources

Ⓔ Fault dimensions and estimates of seismic moments were obtained from published studies and are fully described in the electronic supplement that accompanies this article. Focal mechanisms and seismic moments of specific events have been obtained either from the Global Centroid Moment Tensor database (http://www.globalcmt.org; last accessed December 2013) or the Swiss Seismological Service database (http://www.seismo.ethz.ch; last accessed December 2013).

Acknowledgments

I would like to thank the Ministry of Science and Techonology (MOST) of Taiwan for the financial support of this research. Constructive reviews by Associate Editor Mark Stirling, Thomas Hanks, and an anonymous reviewer improved the quality of the original manuscript.

References

Akaike, H. (1974). A new look at the statistical model identification, *Trans. Auto. Contr.* **AC19,** 716–723.

Allmann, B. P., and P. M. Shearer (2009). Global variations of stress drop for moderate to large earthquakes, *J. Geophys. Res.* **114,** no. B01310, doi: 10.1029/2008JB005821.

Baumont, D., O. Scotti, F. Courboulex, and N. Melis (2004). Complex kinematic rupture of the M_w 5.9, 1999 Athens earthquake as revealed by the joint inversion of regional seismological and SAR data, *Geophys. J. Int.* **158,** 1078–1087, doi: 10.1111/j.1365-246X.2004.02374.x.

Benetatos, C., D. Dreger, and A. Kiratzi (2007). Complex and segmented rupture associated with the 14 August 2003 M_w 6.2 Lefkada, Ionian islands, earthquake, *Bull. Seismol. Soc. Am.* **97,** 35–51, doi: 10.1785/0120060123.

Bodin, P., and J. N. Brune (1996). On the scaling of slip with rupture length for shallow strike-slip earthquakes: Quasi-static models and dynamic rupture propagation, *Bull. Seismol. Soc. Am.* **86,** 1292–1299.

Bouchon, M., M. N. Toksöz, H. Karabulut, M.-P. Bouin, M. Dietrich, M. Aktar, and M. Edie (2002). Space and time evolution of rupture and faulting during the 1999 İzmit (Turkey) earthquake, *Bull. Seismol. Soc. Am.* **92,** 256–266.

Calderoni, G., A. Rovelli, G. Milana, and G. Valensise (2010). Do strike-slip faults of Molise, central-southern Italy, really release a high stress? *Bull. Seismol. Soc. Am.* **100,** 307–324, doi: 10.1785/0120090046.

Chiaraluce, L., W. L. Ellsworth, C. Chiarabba, and M. Cocco (2003). Imaging the complexity of an active normal fault system: The 1997 Colfiorito (central Italy) case study, *J. Geophys. Res.* **108,** 2294, doi: 10.1029/2002JB002166.

Hardebeck, J. L., and A. Aron (2009). Earthquake stress drops and inferred fault strength on the Hayward fault, east San Francisco Bay, California, *Bull. Seismol. Soc. Am.* **99,** 1801–1814.

Hanks, T. C., and W. H. Bakun (2002). A bilinear source-scaling model for **M**– log *A* observations of continental earthquakes, *Bull. Seismol. Soc. Am.* **92,** 1841–1846.

Hanks, T. C., and W. H. Bakun (2008). **M**– log *A* observations for recent large earthquakes, *Bull. Seismol. Soc. Am.* **98,** 490–494, doi: 10.1785/0120070174.

Hanks, T. C., and H. Kanamori (1979). A moment magnitude scale, *J. Geophys. Res.* **84,** 2348–2350.

Hofstetter, A., and A. Shapira (2000). Determination of earthquake energy release in the eastern Mediterranean region, *Geophys. J. Int.* **143,** 898–908.

King, G. C. P., and S. G. Wesnousky (2007). Scaling of fault parameters for continental strike-slip earthquakes, *Bull. Seismol. Soc. Am.* **97,** 1833–1840, doi: 10.1785/0120070048.

Lay, T., and T. Wallace (1995). *Global Modern Seismology*, Academic Press, New York.

Manighetti, I., M. Campillo, S. Bouley, and F. Cotton (2007). Earthquake scaling, fault segmentation, and structural maturity, *Earth Planet. Sci. Lett.* **253,** 429–438, doi: 10.1016/j.epsl.2006.11.004.

Margaris, B. N., and D. M. Boore (1998). Determination of $\Delta\sigma$ and κ_0 from response spectra of large earthquakes in Greece, *Bull. Seismol. Soc. Am.* **88,** 170–182.

Melis, N. S., and K. I. Konstantinou (2006). Real-time seismic monitoring in the Greek region: An example from the 17 October 2005 East Aegean Sea earthquake sequence, *Seismol. Res. Lett.* **77,** 364–370.

Mohammadioun, B., and L. Serva (2001). Stress drop, slip type, earthquake magnitude and seismic hazard, *Bull. Seismol. Soc. Am.* **91,** 694–707.

Pegler, G., and S. Das (1996). Analysis of the relationship between seismic moment and fault length for large crustal strike-slip earthquakes between 1977–92, *Geophys. Res. Lett.* **23,** 905–908.

Rodriguez-Péres, Q., and L. Ottomöller (2013). Finite-fault scaling relations in Mexico, *Geophys. J. Int.* **193,** 1570–1588, doi: 10.1093/gji/ggt050.

Romanowicz, B. (1992). Strike-slip earthquakes on quasi-vertical transcurrent faults: Inferences for general scaling relations, *Geophys. Res. Lett.* **19,** 481–484.

Rovelli, A., and G. Calderoni (2014). Stress drops of the 1997–1998 Colfiorito, central Italy earthquakes: Hints for a common behavior of normal faults in the Appenines, *Pure Appl. Geophys.* doi: 10.1007/s00024-014-0856-1.

Scholz, C. H. (1982). Scaling laws for large earthquakes: Consequences for physical models, *Bull. Seismol. Soc. Am.* **72,** 1–14.

Shaw, B. E. (2009). Constant stress drop from small to great earthquakes in magnitude–area scaling, *Bull. Seismol. Soc. Am.* **99,** 871–875, doi: 10.1785/0120080006.

Shaw, B. E., and S. G. Wesnousky (2008). Slip-length scaling in large earthquakes: The role of deep-penetrating slip below the seismogenic layer, *Bull. Seismol. Soc. Am.* **98,** 1633–1641, doi: 10.1785/0120070191.

Sørensen, M., M. Spada, A. Babeyko, S. Wiemer, and G. Grünthal (2012). Probabilistic tsunami hazard in the Mediterranean Sea, *J. Geophys. Res.* **117,** no. B01305, doi: 10.1029/2010JB008169.

Stirling, M., T. Goded, K. Berryman, and N. Litchfield (2013). Selection of earthquake scaling relationships for seismic-hazard analysis, *Bull. Seismol. Soc. Am.* **103,** 2993–3011, doi: 10.1785/0120130052.

Umutlu, N., K. Koketsu, and C. Milkereit (2004). The rupture process during the 1999 Düzce, Turkey, earthquake from joint inversion of teleseismic and strong-motion data, *Tectonophysics* **391,** doi: 10.1016/j.tecto.2004.07.019.

Waldhauser, F., and W. L. Ellsworth (2000). A double-difference earthquake location algorithm: Method and application to the northern Hayward fault, California, *Bull. Seismol. Soc. Am.* **90,** 1353–1368.

Wells, D. L., and K. J. Coppersmith (1994). New empirical relationships among magnitude, rupture length, rupture width, rupture area and surface displacement, *Bull. Seismol. Soc. Am.* **84,** 974–1002.

Wyss, M. (1979). Estimating maximum expectable magnitude of earthquakes from fault dimensions, *Geology* **7,** 336–340.

Yalcinkaya, E., A. Pinar, O. Uskuloglu, S. Tekebas, and B. Firat (2012). Selecting the most suitable rupture model for the stochastic simulation of the 1999 İzmit earthquake and prediction of peak ground motions, *Soil Dynam. Earthq. Eng.* **42,** 1–16, doi: 10.1016/j.soildyn.2012.05.018.

Yen, Y.-T., and K.-F. Ma (2011). Source-scaling relationship for M 4.6–8.9 earthquakes, specifically for earthquakes in the collision zone of Taiwan, *Bull. Seismol. Soc. Am.* **101,** 464–481, doi: 10.1785/0120100046.

Zahradnik, J., A. Serpetsidaki, E. Sokos, and G.-A. Tselentis (2005). Iterative deconvolution of regional waveforms and a double event interpretation of the 2003 Lefkada earthquake, *Bull. Seismol. Soc. Am.* **95,** 159–172.

Department of Earth Sciences
National Central University
Jhongli 320, Taiwan
kkonst@ncu.edu.tw

Manuscript received 11 March 2014;
Published Online 26 August 2014